Plant Physiology and Biochemistry 194 (2023) 236–245

Contents lists available at ScienceDirect

Plant Physiology and Biochemistry

journal homepage: www.elsevier.com/locate/plaphy

Arabidopsis thaliana sirtuins control proliferation and glutamate dehydrogenase activity

Giovannella Bruscalupi [a], Patrizio Di Micco [b,1], Cristina Maria Failla [c], Gianmarco Pascarella [b,d], Veronica Morea [d], Michele Saliola [a], Angelo De Paolis [e], Sabrina Venditti [a], Maria Luisa Mauro [a,*]

[a] Department of Biology and Biotechnology "Charles Darwin", Sapienza University of Rome, Piazzale A. Moro 5, 00185, Rome, Italy
[b] Department of Biochemical Sciences "A. Rossi Fanelli", Sapienza University of Rome, Piazzale A. Moro 5, 00185, Rome, Italy
[c] IDI-IRCCS, Laboratory of Experimental Immunology, Via dei Monti di Creta 104, 00167, Rome, Italy
[d] National Research Council of Italy, Institute of Molecular Biology and Pathology, Sapienza University of Rome, Piazzale A. Moro 5, 00185, Rome, Italy
[e] Institute of Sciences of Food Production (ISPA-CNR), Via Monteroni, Lecce, 73100, Italy

ARTICLE INFO

Keywords:
Sirtuins
Arabidopsis thaliana
Proliferation
Glutamate dehydrogenase
Sirtuin 3D models

ABSTRACT

Sirtuins are part of a gene family of NAD-dependent deacylases that act on histone and non-histone proteins and control a variety of activities in all living organisms. Their roles are mainly related to energy metabolism and include lifetime regulation, DNA repair, stress resistance, and proliferation. A large amount of knowledge concerning animal sirtuins is available, but data about their plant counterparts are scarce. Plants possess few sirtuins that have, like in animals, a recognized role in stress defense and metabolism regulation. However, engagement in proliferation control, which has been demonstrated for mammalian sirtuins, has not been reported for plant sirtuins so far. In this work, *srt1* and *srt2 Arabidopsis* mutant seedlings have been used to evaluate *in vivo* the role of sirtuins in cell proliferation and regulation of glutamate dehydrogenase, an enzyme demonstrated to be involved in the control of cell cycle in SIRT4-defective human cells. Moreover, bioinformatic analyses have been performed to elucidate sequence, structure, and function relationships between *Arabidopsis* sirtuins and between each of them and the closest mammalian homolog. We found that cell proliferation and GDH activity are higher in mutant seedlings, suggesting that both sirtuins exert a physiological inhibitory role in these processes. In addition, mutant seedlings show plant growth and root system improvement, in line with metabolic data. Our data also indicate that utilization of an easy to manipulate organism, such as *Arabidopsis* plant, can help to shed light on the molecular mechanisms underlying the function of genes present in interkingdom species.

1. Introduction

The sirtuin family comprises highly conserved NAD-dependent enzymes with broad cellular functions, including life span regulation, DNA repair, metabolism, stress resistance, proliferation and energy production (Chang and Guarente, 2014; Carafa et al., 2016). These functions result from sirtuin ability to remove a large array of acyl modifications from cell proteins. Most sirtuins act as deacetylases of histone and non-histone proteins, and some of them show additional enzymatic activities (Bheda et al., 2016). Since these enzymes are regulated by NAD availability, and hence by cell nutritional state, they play important roles in growth and development as well. Protein substrates have been identified for many sirtuins, especially those involved in energy metabolism or stress defence.

Seven members of the sirtuin family have been found in mammals. All of them share a conserved NAD^+ binding catalytic domain, but differ in subcellular localization, enzymatic activity and function. SIRT1, SIRT6 and SIRT7 are predominantly located in the nucleus; SIRT2 is both in the nucleus and in the cytoplasm; SIRT3, SIRT4 and SIRT5 are primarily present in mitochondria (Carafa et al., 2016). Mammalian sirtuin function can vary depending on the tissue taken into consideration. Each organ has unique metabolic pathways and energy sources, showing flexibility in the use of different types of fuels in response to

* Corresponding author.
E-mail addresses: giovannella.bruscalupi@fondazione.uniroma1.it (G. Bruscalupi), patrizio.dimicco@icr.ac.uk (P. Di Micco), c.failla@idi.it (C.M. Failla), gianmarco.pascarella@uniroma1.it (G. Pascarella), veronica.morea@cnr.it (V. Morea), michele.saliola@uniroma1.it (M. Saliola), angelo.depaolis@ispa.cnr.it (A. De Paolis), sabrina.venditti@uniroma1.it (S. Venditti), marialuisa.mauro@uniroma1.it (M.L. Mauro).
[1] Current address: Department of Data Science - The Institute of Cancer Research, London SM2 5NG, United Kingdom.

https://doi.org/10.1016/j.plaphy.2022.11.007
Received 20 June 2022; Received in revised form 4 November 2022; Accepted 6 November 2022
Available online 11 November 2022

Abbreviations

αKG	alpha-ketoglutarate
AtSRT	*Arabidopsis thaliana* sirtuin
BLAST	basic local alignment search tool
DAS	day after seeding
GAS41	glioma-amplified sequence 41 (protein)
GDH	glutamate dehydrogenase
H3K9	histone H3 lysine 9
HsSIRT	*Homo sapiens* sirtuin
NAC	nicotinamide
NAD	nicotinamide adenine-dinucleotide
OsSRT	*Oryza sativa* sirtuin
PAGE	polyacrylamide gel electrophoresis
PDB	protein data bank
RMSD	root-mean square deviation
SIRT	mammalian sirtuin
SRT	plant sirtuin
TCA	tricarboxylic acid
WT	wild type

nutrient availability (Dittenhafer-Reed et al., 2015). Among the numerous described functions, all mammalian sirtuins are involved in the control of cell proliferation in many tumours and stem cells (O'Callaghan and Vassilopoulos, 2017; Fang et al., 2019), although in some cases contrasting effects have been evidenced. SIRT4 acts as a tumour suppressor, whereas SIRT1, SIRT6, SIRT2 and SIRT3 can behave as either suppressors or promoters, depending on cellular context and tumour type (Carafa et al., 2019). SIRT4 was shown to inhibit cell proliferation by regulating glutamine metabolism and its anaplerotic role in the tri-carboxylic acid (TCA) cycle (Jeong et al., 2013; Csibi et al., 2013; Chen et al., 2019). A proposed target of this sirtuin is the enzyme glutamate dehydrogenase (GDH), which catalyses the transformation of glutamate to alpha-ketoglutarate (αKG), an intermediate of the TCA cycle. SIRT4 was shown to inhibit GDH activity by ADP-ribosylation (Haigis et al., 2006). Conversely, other sirtuins, such as SIRT3 and SIRT5, can induce GDH by deacetylation (Schlicker et al., 2008) and deglutarylation (Wang et al., 2018), respectively. SIRT4 inhibition of GDH activity has been proposed to play a role also in DNA damage response, since it results in a slowing down of the TCA cycle and DNA synthesis, thus allowing cells to repair DNA damage (Jeong et al., 2013).

In plant, several studies have underlined the complex and multiple roles of GDH related to developmental process, energy metabolism and stress defence (Dubois et al., 2003). This enzyme has also been suggested to act as a sensor of the carbon/nitrogen status of the plant cell (Tercè-Laforgue et al., 2015). It is of interest to highlight that GDH intersecates many pathways not necessarily correlated to each other and in part still elusive.

Sirtuins have been identified also in plants and shown to have different enzymatic activity and localization, but the actual function has not been demonstrated for all of them (Zheng, 2020). Differently from mammals, only a few sirtuins have been described in each plant species thus far, ranging from four in soybean (*Glycine max*) to two in most of the other species (Zheng, 2020). Plant sirtuins have been studied mainly in *Arabidopsis thaliana* and *Oryza sativa*, in both of which only two genes have been detected.

Based on the analysis of conserved domain regions, AtSRT1 and AtSRT2 gene products have been reported to belong to class II and class IV within the sirtuin family, and to have highest sequence similarity with human SIRT6 (HsSIRT6) and SIRT4 (HsSIRT4), respectively (Pandey et al., 2002). AtSRT1 and AtSRT2 exert deacetylase activity (Hollender and Liu, 2008) but no other enzymatic activity has been described so far. Deacetylase activity has been detected for OsSRT1 and OsSRT2 (Huang et al., 2007; Zhong et al., 2013) as well. Moreover, histone decrotonylation activity has been reported for OsSRT1 (Lu et al., 2018).

In both *Arabidopsis* and rice, AtSRT1 and OsSRT1 are mainly localized in the nucleus (Huang et al., 2007; Liu et al., 2017), and AtSRT2 and OsSRT2 in mitochondria (König et al., 2014), although nuclear localization of AtSRT2 has also been reported (Wang et al., 2010).

The functions of plant sirtuins are far from being completely clarified. OsSRT1 directly regulates H3K9 acetylation and the expression of genes that are related to stress response and metabolism (Zhong et al., 2013). OsSRT1 represses glycolysis by regulating histone modification and inhibiting the moonlighting function of GAPDH, a transcriptional activator of glycolysis, by directly deacetylating the protein (H. Zhang et al., 2017). Down-regulation of OsSRT1 has been shown to enhance histone H3K9 acetylation on transposable elements and on promoters of hypersensitive response-related genes, leading to DNA fragmentation and cell death (Huang et al., 2007). Moreover, OsSRT1 overexpression provides tolerance to oxidative stress, suggesting that it plays a role in both genome stability and redox balance (Huang et al., 2007). Like OsSRT1, AtSRT1 deacetylates and represses several genes involved in plant stress response (Liu et al., 2017). Further, AtSRT1 regulates primary metabolism by modulating the transcriptional factor AtMBP-1 by direct lysine-deacetylation of the protein (Liu et al., 2017). AtSRT2 is likely to play a role in energy metabolism, since it directly deacetylates mitochondrial proteins such as ATP synthase and ADP/ATP carriers (König et al., 2014). Moreover, a negative role in plant basal defence has been proposed, since AtSRT2 expression is downregulated in response to infection with the tomato pathogen, *Pseudomonas syringae* pv. tomato DC3000 (Wang et al., 2010). The two plant sirtuins are usually involved in different and independent processes, but in at least one study they have been reported to work together in the same metabolic pathway, by interacting with the ENAP1 factor and mediating ethylene-induced transcriptional repression by H3K9 deacetylation (Zhang et al., 2018). Therefore, data available so far only suggest that plant sirtuins, like animal homologs, play a role in metabolic pathways related to energy production.

Based on sequence similarity between AtSRT1 and SIRT6, and between AtSRT2 and SIRT4, we hypothesized that *Arabidopsis* sirtuins play a role like that of the human enzymes, which are engaged in the control of proliferation. To date, no information about specific involvement of plant sirtuins in this pathway is available. To evaluate this hypothesis, we utilized *Arabidopsis* mutants *srt1* and *srt2*, lacking the SRT1 and SRT2 gene, respectively.

In parallel, bioinformatics analyses were performed to investigate in detail the sequence and structure similarities between *Arabidopsis* SRT1 and SRT2 proteins and between each of them and human SIRT6 and SIRT4. These analyses showed that AtSRT1 and AtSRT2 are highly conserved with respect to HsSIRT6 and HsSIRT4 in terms of 3D structures and functional residues, as well as of sequences, and indicate that vegetable sirtuins are more closely related to each other than SIRT6 is to SIRT4.

In vivo analysis of *srt1* and *srt2* plants demonstrated increased DNA synthesis in both mutants with respect to wild-type (WT) plants, suggesting sirtuin engagement in cell proliferation control, which we propose to be mediated by the inhibition of GDH activity, as previously reported for mammalian SIRT4 (Jeong et al., 2013). These metabolic data corroborate the phenotypic parameters observed in *Arabidopsis* mutant seedlings.

2. Materials and methods

2.1. Bioinformatics analysis of sirtuin sequences and structures

The amino acid sequences of AtSRT1 and AtSRT2 proteins and of their human homologs HsSIRT6 and HsSIRT4 were downloaded from the UniProt web site (https://www.uniprot.org/).

The BLAST program (Altschul et al., 1997) was used for pair-wise sequence comparisons, and to search NCBI sequence databases for sequences homologous to those given as input. ClustalO (Sievers et al., 2011) was used to generate multiple sequence alignments.

The publicly available 3D structures of HsSIRT6 were downloaded from the Protein Data Bank (PDB; rcsb.org) (Berman et al., 2000). The 3D atomic models of AtSRT1, AtSRT2, HsSIRT4 and HsSIRT6 were downloaded from the AlphaFold Protein Structure Database (https://alphafold.ebi.ac.uk/) (Jumper et al., 2021).

Structure visualization, superposition and analysis were carried out using the Chimera program (Pettersen et al., 2004). Structure comparisons were performed with Chimera and structural searches in the PDB were performed using the Protein structure comparison service PDBeFold at the European Bioinformatics Institute (http://www.ebi.ac.uk/msd-srv/ssm). Structurally conserved regions are defined as the largest regions comprising residue pairs whose Cα-Cα distance is $\leq$ 2.5 Å. Two residues are defined to be in contact if they comprise at least one atom at a distance $\leq$4.0 Å from one of the atoms of the other residue.

2.2. Plant material and growth conditions

All experiments were performed using *Arabidopsis* ecotype Columbia (Col. 0). Seeds from WT and both SRT1 and SRT2 mutant plants were surface sterilized, plated on solid medium (1/2 Murashige and Skoog (MS) medium, 1% sucrose, 0.8% agar, pH 5.7) and cold-treated for 2 days to break dormancy and synchronize germination. MS medium was from Duchefa (Haarlem, The Netherlands) and agar (Agar-Agar) was from Merck (Darmstadt, Germany). Experiments were performed in plate-cultured seedlings, grown both horizontally and vertically. To obtain mutant homozygotes, plants were placed in 13-cm clay pots containing Metro-Mix (W.R. Grace & Co.) in a chamber at 24/21 °C under long-day conditions, with 16/8 h day/night cycles and light intensity of 300 μmol m^{-2} s^{-1}.

2.3. Isolation of srt1 and srt2 homozygous plants

Seed mutants for *SRT1* Salk-001493 (locus At5G55760) and *SRT2* Salk-149295 (locus At5G9230) were selected from a Salk library relative to T-DNA insertion, and a screening by PCR analysis was performed to search for homozygotic plants.

Primers corresponding to T-DNA border LBb1.3 ATT TTG CCG ATT TCG GAA C and primers corresponding to SRT1 (forward 5′-CGCAGAGAGAGAACAAAATCG-3′ and reverse 5′-TTCCACATTCTGTGCTAACCC-3′) and SRT2 (forward 5′-GTT TCG CTT GAC ACA TGT TCC-3′and reverse 5′-GAGAACAGCACGAAACGAAAC-3′) were produced to carry out PCR analysis. Primers utilized for actin2 gene as control are: forward 5′- CTAGGATCCAAAATGGCCGATGGTGAGG-3′ and reverse 5′-GAAACTCACCACCACGAACCAG-3'. A number of positive lines were identified for each homozygote mutant. Line #4 for SRT1 and line #2A for SRT2 were utilized for all the experiments. Absence or presence of RNA expression were verified by qPCR analysis.

2.4. Real-time RT-PCR

To evaluate levels of SRT1 and SRT2 mRNA expression in mutant samples, real-time RT-PCR was performed. Total RNA was extracted from plant tissue and cDNA was obtained using Superscript III First Strand System (Invitrogen, Carlsbad, CA, USA), according to the manufacturer's protocol. Real-time RT-PCR was performed by the dual-labelled fluorogenic probe method, using ABI Prism 7000 sequence detector (PerkinElmer, Groningen, The Netherlands). Expression levels were calculated by the relative standard curve methods. Primers used were: SRT1 forward 5′-AAAGCCTGAGAGAGAAAGCG-3′ and reverse 5′-AACAGCCTCACTTCTCGGTT-3'; SRT2 forward 5′-CATGAGGCTGGTGCTATGAC-3′ and reverse 5′-CCACGTCAAGAACTCTGTGC-3'. Experiments were repeated at least three times with comparable results.

2.5. Cell proliferation analysis

DNA synthesis rate was determined using ^{3}H thymidine *in vivo* incorporation assay described by Baiza et al. (1989) with minor modifications. Pools of almost 20 whole plants at 10 or 15 days after seeding (DAS) were dipped in 2 ml of MS/2 culture medium (Duchefa, Haarlem, The Netherlands) supplemented with 1 μCi ^{3}H-methyl-thymidine. Following 4 h incubation, plants were thoroughly rinsed with 1% Na-citrate, and subsequently with 95% ethanol. All solutions contained 200 μg/ml of unlabelled thymidine. Rinsed plants were homogenized in 1 ml 95% ethanol. DNA was extracted and purified (Baiza et al., 1989), and the incorporated radioactivity was determined by liquid scintillation counting in a Packard TRI-CARB 2100 TR.

2.6. GDH activity assay

GDH (EC 1.4.1.2) activity was assayed on extracts of whole fresh pooled plants or separated roots and shoots. The extracts were obtained as reported by Turano et al. (1997). Materials (approximately 300 mg) were ground to powder in liquid nitrogen, transferred into 400 μl of extraction buffer (50 mM Tris-HC1, pH 8.0, 1 mM EDTA, 5% [v/v] glycerol, 0.05% [v/v] Triton X-100, and 0.5% [w/v] PVP-40) and incubated on ice for 30 min. Samples were centrifuged at 13,000g for 10 min to remove debris. Protein concentration of the extracts was determined by the method of Lowry et al. (1951).

In vitro NAD-dependent GDH activity was evaluated in the extracts as reported by Groat and Vance (1981). The reaction buffer contained 80 mM L-glutamic acid and 0.2 mM NAD in 50 mM Tris-HCl buffer (pH 8.8), in a final 1 ml volume. The reaction was initiated by adding 100 μl of plant extract (100 μg protein) to the reaction buffer. NAD reduction was spectrophotometrically measured at 340 nm for 7 min. Enzymatic activity, expressed as nmol of reduced NAD/min/ml, was calculated using NAD extinction coefficient at 340 nm.

For *in gel* GDH activity determination, extracts were subjected to native PAGE with 5% acrylamide gel in a Mighty small SE 250 Hoefer Minigel electrophoresis (Scientific Instruments). Equal amounts of extract proteins (28 μg) in loading 4X buffer (Tris-HCl pH 6.8100 mM, glycerol 50%, 2-Mercaptoethanol 20 mM, Bromophenol blue 0.002%) were run at 20 mA constant current at 4 °C. Protein bands showing GDH activity were visualized by gel incubation under shaking conditions in 5 ml of deionized water containing 50 μl glutamate (100 mg/ml), 25 μl NAD (100 mg/ml), 25 μl nitrobluetetrazolium (50 mg/ml) and 10 μl phenazinemethosulfate (40 mg/ml) at room temperature until activity was detected (Marchi et al., 2013). Band intensity was calculated using ImageJ software.

2.7. Plant weight determination

srt1 and *srt2* mutants and WT seedlings were horizontally grown in plates at 24/21 °C, 16h light, 8h dark. Plant weight evaluation was carried out at 10 and 15 DAS. For each genotype, a pool of 20 seedlings was used in at least ten biological replicates.

2.8. Root analysis

Plants were vertically cultured in plates with MS/2 medium and 8% agar, in a conditioned chamber at 24/21 °C, 16h light, 8h dark. Root growth analysis was carried out by measuring the length (mm) of primary roots at 10 and 15 DAS in at least 20 seedlings for each phenotype. The analysis was repeated ten times.

2.9. Statistical analysis

Student's t-test was used to evaluate statistical significance of results

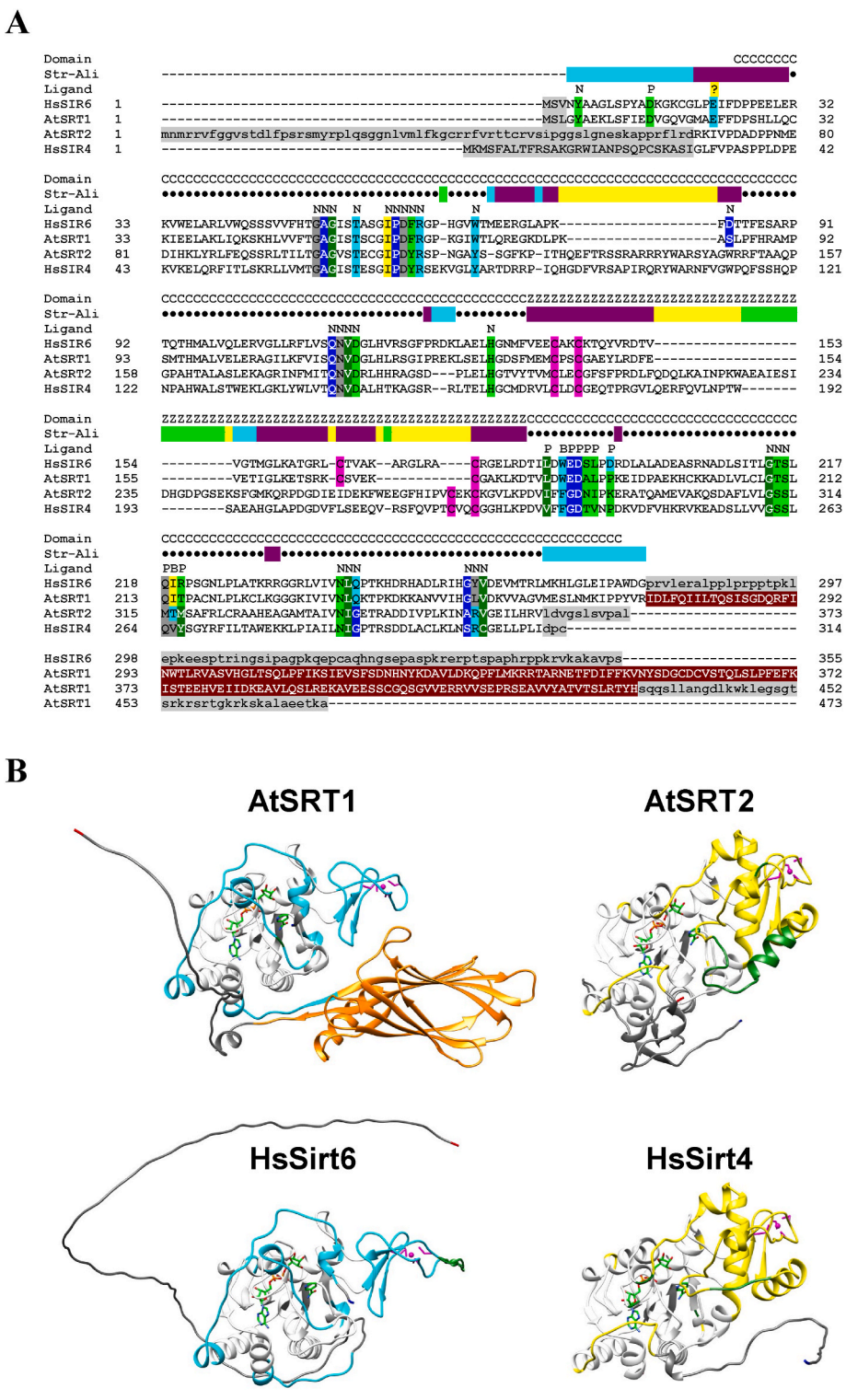

Fig. 1. A. Structure-based sequence alignment between AtSRT1, AtSRT2, HsSirt6 and HsSirt4. Amino acids are indicated by one-letter code, and sequence numbering is reported at the beginning and end of each sequence block. HsSirt6 residues are colour-coded based on the type of interaction that they establish with ADP-ribose, NCA and/or peptide substrate in one or more of the experimentally determined HsSirt6 structures, as follows: cyan and blue, polar interactions (i.e., salt-bridges or hydrogen bonds) involving side-chain and main-chain atoms, respectively; yellow, van der Waals interactions between hydrophobic atoms; light and dark green, both hydrophobic and polar interactions, involving side-chain and main-chain atoms, respectively; grey, van del Waals interactions between polar and hydrophobic atoms. HsSirt4, AtSRT1 and AtSRT2 residues are colour-coded like HsSirt6 if they are predicted to have conserved main-chain conformation and comprise chemical groups able to establish polar or van der Waals interactions with ADP-ribose, NCA and/or peptide ligands. Additionally, in all sequences, zinc-binding cysteine residues are coloured magenta; residues belonging to AtSRT1 unique Ig-like domain are dark red; unstructured regions external to the structurally conserved ones, namely, N-terminal regions of AtSRT2 and HsSirt4 and C-terminal regions of AtSRT1 and HsSirt6, are grey. In the "Domain" rows, "C" and "Z" upper-case letters indicate residues belonging to the catalytic and Zn-binding domain, respectively. In the "Str-Ali" (i.e., Structurally Aligned) rows, "●" symbol, cyan, yellow and purple indicate regions that are structurally conserved among all four proteins, between AtSRT1 and HsSirt6, between AtSRT2 and HsSirt4, both between AtSRT1 and HsSirt6 and between AtSRT2 and HsSirt4 (but not between any member of the first pair and any member of the second pair), respectively; green indicates residues are not structurally conserved but are comprised between conserved regions. In the "Ligand" rows, "N", "P" and "B" upper-case letters below the horizontal bars indicate residues involved in interactions with ligands deriving from NAD hydrolysis (i.e., ADP-ribose and NCA), peptide substrates or both, respectively.
B. Molecular models built for AtSRT1, AtSRT2, HsSirt6 and HsSirt4. The Cα carbon atoms are shown as ribbons and coloured white, cyan, yellow, green and grey according to structural conservation, as in the horizontal bars above the sequence alignment in the top panel; additionally, residues belonging to the AtSRT1 unique Ig-like domain are orange, and the unstructured AtSRT2 and HsSirt4 N-terminal regions and AtSRT1 and HsSirt6 C-terminal regions are grey. N-terminal and C-terminal residues are blue and red, respectively. The side-chains of zinc-binding cysteine residues are shown as sticks and the zinc atoms as a magenta-coloured sphere. The ADP-ribose and NCA moieties deriving from the hydrolysis of the NAD cofactor are shown as stick and coloured by atom-type: C, green; O, red; N, blue; P, orange.

in qPCR, cell proliferation, GDH activity, fresh weight, and root length measurement.

3. Results

3.1. Bioinformatics analysis of Arabidopsis and human sirtuins

3.1.1. Sequence analysis

AtSRT1 (UniProt ID: Q9FE17) and AtSRT2 (UniProt ID: Q94AQ6) protein sequences comprise 473 and 376 amino acids (a.a.), respectively. Pairwise BLAST alignment of the two sequences encompasses 293 residues with 28% sequence identity and 20% insertions or deletions (Supplementary Fig. 1), suggesting that they are distantly related to each other, in agreement with Pandey et al. (2002).

The closest human homologs of AtSRT1 and AtSRT2, namely HsSIRT6 (UniProt ID: Q8N6T7) and HsSIRT4 (UniProt ID: Q9Y6E7), respectively, comprise 355 a.a. and 314 a.a., respectively. The E-values and percentage of sequence identity between each of the *A. thaliana*

Table 1
Pairwise comparisons of AtSRT1, AtSRT2, HsSIRT6 and HsSIRT4 3D models and sequences over the longest structurally conserved regions in each pair of proteins. Root-mean square deviation (RMSD) values (in Å) calculated after optimal pairwise superpositions of Cα atoms, are followed by the length of the structurally conserved regions, in parenthesis. Percentages of sequence identity are followed by the number of identical residues *vs.* the number of structurally aligned residues, in parenthesis.

	AtSRT1	AtSRT2	HsSirt6	HsSirt4
AtSRT1	–	1.12 Å (143)	0.81 Å (269)	1.17 Å (166)
AtSRT2	42% (60/143)	–	1.16 Å (171)	0.92 Å (275)
HsSirt6	51% (138/269)	37% (63/171)	–	1.23 Å (178)
HsSirt4	37% (61/166)	44% (122/275)	34% (60/178)	–

sirtuins and each of their human homologs are reported in Supplementary Table 1.

In the ClustalO generated multiple sequence alignment of the four proteins (Supplementary Fig. 2), about 250 residues are aligned. Most of the aligned residues are located within the catalytic domain region (see below), and 109 residues (*i.e.*, 43%) are identical in all four proteins. In addition to the aligned regions, AtSRT2 contains a longer N-terminal sequence, and AtSRT1 and HsSirt6 have longer C-terminal tails, respectively.

3.1.2. Structure analysis

Several 3D structures of HsSIRT6, determined by X-ray crystallography, are available from the PDB (see Supplementary Table 2). These encompass from 285 to 298 HsSIRT6 residues within the 1–298 region, out of the 355 residues comprised in HsSIRT6. Conversely, the 3D structures of HsSIRT4, AtSRT1, AtSRT2 and of the 57-residues in the C-terminal HsSIRT6 region have not been experimentally determined. To perform structure analyses, we used the atomic models of all the four proteins built by AlphaFold2 (Fig. 1), which has been recently demonstrated to largely outperform all other protein structure prediction methods and produce models of accuracy comparable to known structures in blind tests (Jumper et al., 2021).

Structural analysis of these models (see Fig. 1) revealed that the conformation of the catalytic domain, which is involved in both NAD cofactor and peptide substrate binding, is largely conserved in all four proteins. Indeed, 169 out of 226 residues (i.e., 75%, indicated by "●" symbol in Fig. 1A, assume similar conformations in all four proteins. This is highlighted by the root-mean square deviation (RMSD) values calculated after optimal superposition of Cα atoms of the 169 structurally aligned residues and the percentage of sequence identity in the same regions, reported in Supplementary Table 3.

At variance with the catalytic domain, the zinc-binding domain assumes two different conformations in the four proteins: one of the two conformations is shared by AtSRT1 and HsSIRT6, and the other conformation is shared by AtSRT2 and HsSIRT4 (see the "Domain" row in Fig. 1A). For this reason, the structurally conserved regions between AtSRT1 and HsSIRT6 (i.e., 269 structurally aligned residues) and between AtSRT2 and HsSIRT4 (i.e., 275 structurally aligned residues) are significantly more extended than the structurally conserved regions among all four proteins (Table 1).

In addition to the catalytic and zinc-binding domains, all four proteins comprise unique regions: i) AtSRT1 contains one additional immunoglobulin (Ig)-like domain (see below) between the catalytic domain and the ~40-residue C-terminal tail, which is predicted to be unstructured; ii) AtSRT2 comprises a ~65-residue N-terminal region predicted to form a three-strand β-sheet with the 10-residue C-terminal tail; iii) HsSIRT4 has a ~30 residues N-terminal region and HsSIRT6 has a ~75 residues C-terminal region, both of which are predicted to be unstructured.

Interestingly, the values reported in Table 1 and Supplementary Table 3 indicate that structure and sequence similarity between AtSRT1 and AtSRT2 is higher than that between HsSIRT6 and HsSIRT4, suggesting that the *Arabidopsis* proteins are more closely related to each other than their human counterparts.

3.1.3. Function analysis

HsSIRT6 residues in contact with ADP-ribose and/or nicotinamide (NCA), which are the molecules deriving from the hydrolysis of the NAD cofactor, and/or with the peptide substrate, comprising either N(6)-acetyl-L-lysine or N(6)-tetradecanoyl-L-lysine, in the experimentally determined HsSIRT6 structures analysed in this work (see Supplementary Table 2), are highlighted in Fig. 1, together with the type of interaction (i.e., polar or non-polar) that they establish with the ligand. In the same Figure, AtSRT1, AtSRT2 and HsSirt4 residues occurring at structurally equivalent positions with respect to those involved in ligand binding in HsSirt6 structures, are coloured based on the type of interaction that they are predicted to establish with the same ligands. A summary of the expected conservation of interactions between each pair of proteins is reported in Table 2. In agreement with results of sequence and structure analysis, AtSRT1 has highest conservation of functional residues with HsSirt6, and AtSRT2 with HsSirt4.

As far as regions external to the conserved core of the catalytic domain are concerned, sequence database searches did not provide indications about their possible function. The unstructured C-terminal tails of either AtSRT1 or HsSirt6 (comprising a.a. 433–473 and 279–355, in the respective sequences) have BLAST-detectable sequence similarity only with sirtuin homologs from Brassicaceae and animal species, respectively. The unstructured N-terminal regions of AtSRT2 and HsSIRT4 (comprising a.a. 1–69 and 1–31, respectively) do not match any *A. thaliana* or human sequence with significant E-values (AtSRT2 matches two human proteins below threshold: estrogen-induced tag 6 and egl nine homolog 2 with 36% sequence identity over 47 residues). Additionally, no experimentally determined 3D structure present in the PDB was detected by the PDBeFold server to have similar conformation to any of these N- or C-terminal sirtuin regions.

Conversely, a structural search in the PDB archive performed by the PDBeFold server using the unique all-β immunoglobulin (Ig)-like domain (a.a. 274–432) of AtSRT1 as query, revealed that this domain is structurally similar to human GAS41 (RMSD value: 1.84 Å over 107 structurally aligned residues between AtSRT1 molecular model and

Table 2
Expected conservation of interactions with ligand molecules (i.e., ADP-ribose, NCA and peptide substrate) between each pair of proteins analysed in this work. Str-Ali, Ide, Sim, Diff: Number of residues that are structurally aligned, identical, expected to establish similar interactions and expected to establish different interactions, respectively.

		Cofactor				Peptide Substrate			
		Str-Ali	Ide	Sim	Diff	Str-Ali	Ide	Sim	Diff
AtSRT1	**HsSirt6**	29	27	2	–	11	8	2	1
AtSRT2	**HsSirt4**	26	24	2	3	10	3	6	2
AtSRT1	**AtSRT2**	26	17	6	6	10	1	6	4
HsSirt6	**HsSirt4**	26	16	7	6	10	2	5	4
AtSRT1	**HsSirt4**	26	16	7	6	10	3	5	3
AtSRT2	**HsSirt6**	26	17	6	6	10	1	6	4

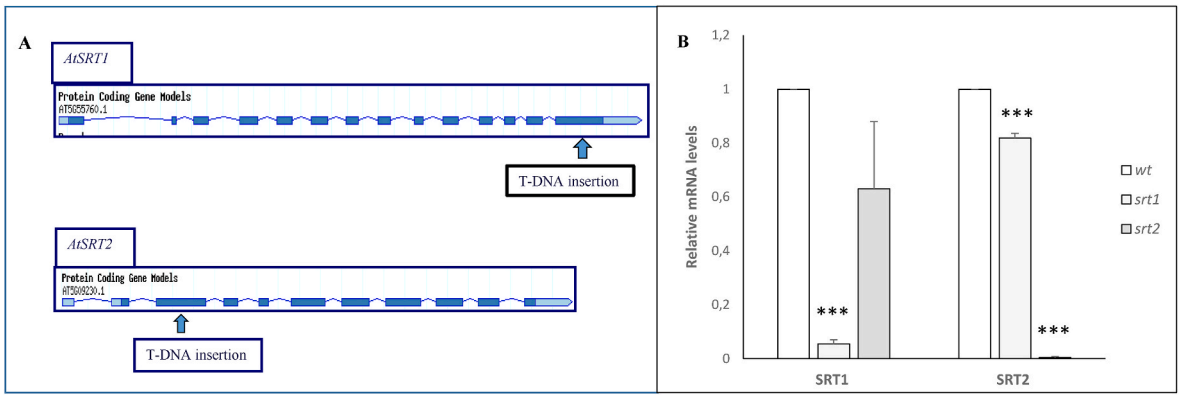

Fig. 2. (A) AtSRT1 and AtSRT2 gene map. The T-DNA insertion site is indicated by the arrow. **(B)** Real-time RT-PCR expression level of AtSRT1 and AtSRT2 in WT and mutant plants. Results are expressed as means ± SD obtained from at least three experiments. mRNA expression in WT plants was assumed to be 1. ***$p < 0.001$.

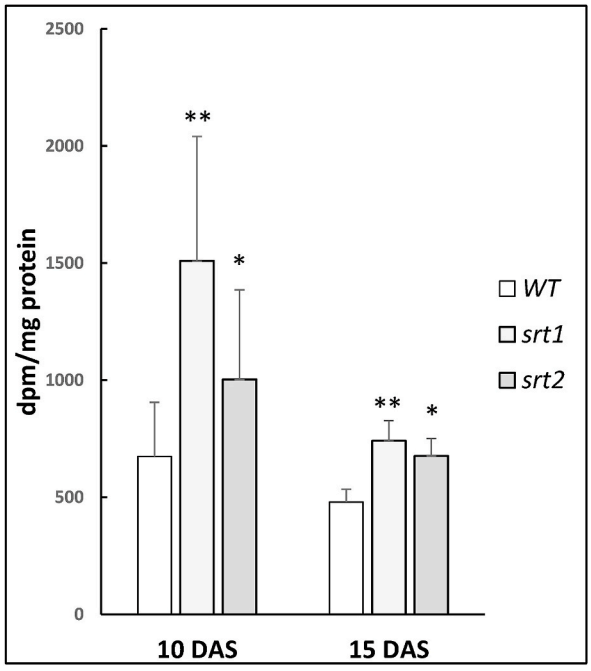

Fig. 3. ^{3}H-thymidine incorporation in whole *A. thaliana* WT, *srt1*mutant and *srt2* mutant. Results at 10 and 15 DAS are expressed as dpm incorporated ^{3}H thymidine/mg protein. Data are the mean ± S.D. of at least 6 experiments. *$p < 0.05$, **$p < 0.01$.

GAS41 3D structure in PDB entry: 5vna, chain D). GAS41 is a chromatin-associated protein belonging to the YEATS family, which is involved in the recognition of acetyl-lysine in histone proteins, with a preference for H3K18 and H3K27 peptides (Cho et al., 2018). GAS41 has been suggested to be a reader of diacetylated histones, since it contains a C-terminal coiled-coil domain that is responsible for protein dimerization, and binds to diacetylated H3 peptides with higher affinity than monoacetylated peptides.

3.2. Mutant sirtuin production

To investigate *Arabidopsis* sirtuin function, plant mutants for *SRT1* and *SRT2* genes were utilized. Two lines, obtained from a Salk library of insertional T-DNA, were used to achieve homozygous seeds, whose production was confirmed by PCR analysis (Fig. 2A). To verify the lack of expression of sirtuin genes, homozygous *srt2* and *srt1* plants were analysed through real-time RT-PCR. The assay demonstrated that *srt2* plants did not express the *SRT2* gene at all (knock-out) while *srt1* plants conserved a slight residual *SRT1* gene expression, ten-fold lower (knock-down) than WT (Fig. 2B). Presence of a mutant sirtuin gene might interfere with the expression of the other one. To explore this possibility, real-time RT-PCR analysis was carried out in both mutant plants. As shown in Fig. 2B, in *srt2* mutants the expression level of SRT1 was partially affected, with a reduction of 37% in respect to WT, whereas SRT2 expression in the *srt1* mutant was 20% lower than WT plants. Therefore, in the plant system, knock-out or knock-down of a sirtuin gene interfered with the expression of the other one.

3.3. Cell proliferation levels in SRT1 and SRT2 mutant plants

The observation that AtSRT1 and AtSRT2 show both structure and sequence similarity with human SIRT6 and SIRT4, prompted us to evaluate the effect of *Arabidopsis* sirtuins on cell proliferation.

DNA synthesis analysis was performed on young seedlings at 10 and 15 DAS, two developmental stages characterized by high cell proliferation rate (Kang and Dengler, 2002; Beemster et al., 2005).

The assay was performed in horizontally cultured whole plants, by estimating the incorporation of radioactive thymidine into the DNA of dividing cells. At both 10 and 15 DAS, enhanced DNA replication was observed in mutant plants. Specifically, at 10 DAS, *srt1* and *srt2* plants showed 200% and 35% activity increase with respect to control plants, respectively. At 15 DAS, DNA synthesis was decreased in all plants compared to 10 DAS, but significant differences were still evident between mutant and control plants (Fig. 3).

This result indicates that both AtSRT1 and AtSRT2 exert an inhibitory role on DNA replication.

3.4. GDH activity in srt1 and srt2 mutant plants

To elucidate the mechanism underlying the inhibitory effect of *Arabidopsis* sirtuins on cell proliferation, we addressed glutamine metabolism.

In condition of carbon restriction, such as those of highly proliferating human cells, glutamine is metabolized to glutamate. Glutamate, in turn, is deaminated to α-ketoglutarate (αKG), which fuels the TCA cycle, thereby providing both energy and metabolites that are necessary for proliferation (Jeong et al., 2013). The enzyme responsible for glutamate deamination is the NAD-dependent GDH. To assess whether the increased proliferation observed in mutant plants is related to glutamine metabolism modifications, we carried out an *in vitro* assay of NAD-dependent GDH activity in protein extracts of WT, *srt1* and *srt2* whole plants at both 10 and 15 DAS.

GDH activity in *srt1* and *srt2* plants was 38% and 42% higher than in WT plants, respectively (Fig. 4A), indicating that both plants produce more αKG. This, in turn, fuels the TCA cycle, thereby increasing DNA

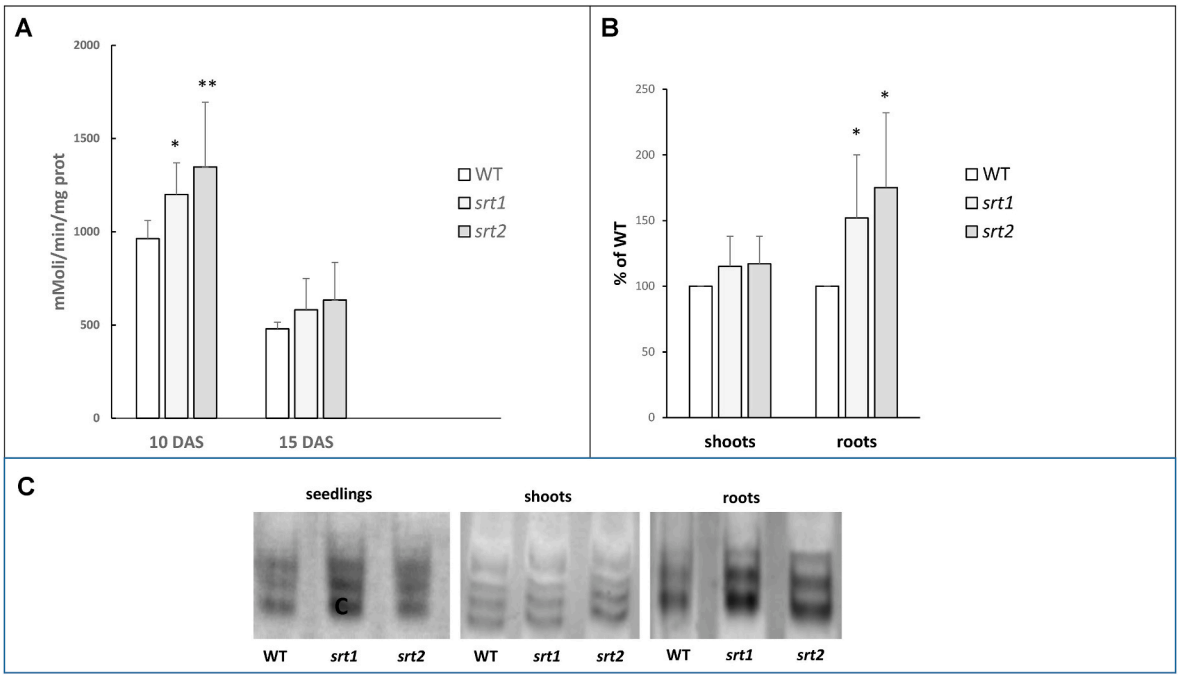

Fig. 4. NAD-dependent GDH enzyme activity in *A. thaliana* WT, *srt1* and *srt2* plants. **(A)** Enzyme activity in seedlings at 10 and 15 DAS. Enzyme activity is expressed as nmol/min/mg protein. *p < 0.05; **p < 0.01. Experiments were repeated 6 times. **(B)** Enzyme activity in shoots and roots at 15 DAS. *p < 0.05. **(C)** GDH isoenzyme pattern at 15 DAS in seedlings, shoots and roots. All assays were repeated in at least three biological replicates.

synthesis.

3.5. GDH activity in srt1 and srt2 shoots and roots

In plants, especially in *Arabidopsis*, GDH is reported to be more active in roots with respect to other organs (Miyashita and Good, 2008). To assess if this was the case in our system conditions, we assayed GDH activity in shoots and roots of WT, *srt1* and *srt2* seedlings at 15 DAS (Fig. 4B).

The obtained data agreed with literature reports, since GDH activity in the root system is most prominent in all examined plants (Fig. 4C). Moreover, root activity was significantly higher in mutant plants; in particular, 40% and 50% rise of GDH activity in *srt1* and *srt2*, respectively, was detected (Fig. 4B). Conversely, enzyme activity in shoots of both mutants was only slightly increased compared with WT.

Therefore, the increased GDH activity observed in whole mutant plants (Fig. 4A) can be ascribed mostly to the root system, and only to a small extent to the shoots.

3.6. GDH isoform pattern

GDH is encoded by three genes, namely *GDH1, GDH2* and *GDH3*, which encode polypeptides beta, alpha and gamma, respectively. These can assemble either as homo- or hetero-hexamers, producing seven isoenzymes (Marchi et al., 2013). The specific isoenzyme pattern is known to vary depending on plant age and tissue (Miyashita and Good, 2008). To compare GDH isoenzyme patterns between mutant and control *Arabidopsis* plants, proteins extracted from whole plants or from shoots and roots separately, were run on non-denaturing PAGE and subjected to *in-gel* staining for NAD-dependent GDH activity. Results showed that the GDH isoenzyme pattern in mutant plants is not different from WT (Fig. 4C). This indicates that sirtuins do not interfere with either the number or activity of enzyme subunits in shoots and roots. The results of the *in-gel* assay parallel those of *in vitro* analysis, since both

A

plant	fresh weight (mg)	
	10 DAS	15 DAS
WT	43.25 ± 3.7	58.00 ± 6.0
srt1	69.75 ± 32.1*	75.50 ± 26.25
srt2	66.25 ± 30.2*	74.25 ± 24.50*

B

plant	primary root lenght (mm)	
	10 DAS	15 DAS
WT	15,4 ± 2.0	22.4 ± 2.1
srt1	18.6 ± 3.1	25.1 ± 3.4*
srt2	21.6 ± 5.1*	27.3 ± 4.9**

Fig. 5. WT, *srt1* and *srt2* seedling phenotype analysis. (A) Fresh weight of horizontally grown seedlings at 10 and 15 DAS for each genotype. (B) Length of vertically grown primary roots at 10 and 15 DAS. (C) Vertically cultured seedlings at 15 DAS. Data are the mean ± S.D. of at least 5 experiments. *p < 0.05, **p < 0.01.

mutant plant roots showed higher enzyme activity with respect to WT, whereas only a slight difference was detected in the shoots.

3.7. srt1 and srt2 seedlings phenotype

To assess whether the lack of sirtuin genes interferes with *Arabidopsis* seedling morphology, *srt1* and *srt2* plants were phenotypically characterized in the same growth conditions used for biochemical experiments. At the selected time points (i.e., 10 and 15 DAS), no obvious developmental alterations were evidenced at the macroscopic level. However, fresh weight evaluation of both *srt1* and *srt2* horizontally cultured plants at 10 and 15 DAS showed higher values than WT. A 30% increment in *srt1* and 40% in *srt2* was observed at 10 DAS (Fig. 5A). To better investigate this aspect, a vertical *in vitro* growth assay of seedlings was settled at 10 and 15 DAS as well, to search for root growth alterations. In these conditions, promotion of primary root length was appreciated in both mutants, in particular at 15 DAS (Fig. 5B–C).

4. Discussion

Plants and animals, even if phylogenetically distant, share genes, biochemical pathways and molecular mechanisms. Since mammalian sirtuins play many essential regulatory functions, it is extremely interesting to understand if, and to what extent, plant sirtuins exert similar roles.

Nearly all the seven sirtuins that have been identified in animal cells are involved in cell proliferation. Conversely, the few available studies on sirtuins that have been consistently described in plant cells until now, indicate that most of their functions are related to energy metabolism and buffering many kinds of stresses, induced by either internal or external environment. However, no information about the involvement of plant sirtuins in cell proliferation has been provided yet.

In this manuscript, we demonstrate that both the *Arabidopsis* sirtuins play a role in cell proliferation control. In fact, by analysing young *Arabidopsis* seedlings at an early developmental stage, which is characterized by high proliferation rate, we found an increment of DNA synthesis in both *srt1* and *srt2* plants, with respect to control plants. This observation is consistent with an inhibitory role of both sirtuins on DNA duplication rate.

We hypothesized that the mechanism underlying this ability may be related to glutamine metabolism since, in animal cells, glutamine has been linked to the cell cycle machinery (J. Zhang et al., 2017). Glutamine can be metabolized to glutamate and this, in turn, to αKG, which can replenish TCA cycle thereby providing both energy and substrates for cell proliferation. In human cells, SIRT4 has been reported to slow down glutamine metabolism through GDH inhibition (Jeong et al., 2013; Csibi et al., 2013). This inhibitory function has been demonstrated only for SIRT4, although several mammalian sirtuins are able to modulate GDH enzymatic activity through different post-translational modifications (Schlicker et al., 2008; Wang et al., 2018).

Here we show, for the first time, that both AtSRT1 and AtSRT2 inhibit *Arabidopsis* GDH activity, as we detected it at higher level in each mutant plant compared with the control. At least in the case of AtSRT2, increased GDH activity is unlikely due to augmented gene transcription since a transcriptome analysis did not highlight significant differences in expression of any of the three GDH genes with respect to WT (our unpublished data). This suggests that sirtuins exert a direct effect on GDH enzymatic activity.

Different GDH activity has been observed depending on plant organ, cell type, physiological state and external environmental conditions. In particular the activity is higher in roots than in shoots (Miyashita and Good, 2008). In agreement with these observations, our data indicate that basal GDH levels are more pronounced in roots in either mutant or WT plants, and that the increment of GDH activity, observed in *srt1* and *srt2*, is mostly confined to this organ. Conversely, no difference in GDH subunit composition was observed between WT and mutant plants, neither in relative intensity nor in subunit number, thus ruling out the possibility that sirtuins influence the levels of specific isoenzymes.

In animal cells, GDH is allosterically regulated by the energetic status of the cell, whereas in plant no evidence of this mechanism has been found (Li et al., 2012). In the light of our findings, it is possible that plant GDH is dependent on sirtuin ability to sense energetic states.

As far as the effect of sirtuins on plant phenotype is concerned, only a few morphological and developmental alterations have been described to date. Some studies have reported early flowering in *Arabidopsis* mutants (Bond et al., 2009), in line with current evidence about epigenetic control of flowering (Wang and Köhler, 2017). Using the sirtuin inhibitor sirtinol, Grozinger et al. observed a modified plant structure at the initial developmental stage in body-axis formation, such as shorter hypocotyls, lack of roots, and epinastic cotyledons. These alterations are like those found in plants presenting an auxin impairment, therefore sirtuins have been suggested to be involved in synthesis, transport or cellular response to this hormone (Grozinger et al., 2001).

In our work, *srt1* and *srt2* young seedlings did not show evident morphological alterations. However, a small increase in plant mass and improvement of root system was detected. The phenotypical boost exhibited by seedlings may be ascribed, at least in part, to the metabolic alterations described in our mutant plants. Indeed, on the one hand, higher rate of DNA synthesis is likely to result in accelerated growth of mutant plants with respect to controls; on the other hand, GDH, known to be a stress responsive enzyme, improves not only tolerance but also growth efficiency in many plants, such as rice, potato, tobacco, *Zea mais* (Tercè-Laforgue et al., 2015). In *Arabidopsis,* Melo Oliveira et al. (1996) showed reduced growth in null GDH1 mutant plants and Miyashita and Good (2008) reported growth retardation in double GDH1 and GDH2 mutants.

Moreover, GDH overexpressing tobacco plants display enhanced root growth and higher yields (Dubois et al., 2003). The biochemical mechanism underlying this process has not been elucidated yet, but it might be related to the role that GDH plays at the crossroad between N and C metabolism, crucial for plant growth. In none of these reports, a direct relationship between GDH and proliferation was described. However, mass increment may be caused by a higher proliferation rate that, in turn, correlates with augmented GDH activity, able to fuel the TCA cycle and thereby increasing cell energy.

To rationalize the effects of AtSRT1 and AtSRT2 on a molecular basis, we took advantage of their close evolutionary relationships with the two human sirtuins HsSIRT6 and HsSIRT4, whose function and, in the case of HsSIRT6, 3D-structure, have been extensively characterized. Bioinformatics analyses indicated that the catalytic domain regions involved in interactions with NAD cofactor and peptide substrates are highly conserved in the four proteins, both in terms of main-chain conformation and of the chemical-physical properties of functional residues, which are only slightly less conserved at positions involved in peptide binding with respect to those interacting with NAD. These results indicate that the four proteins are likely able to bind the same, or similar peptides, and catalyse the same de-acylation and ADP-ribosylation reactions demonstrated for HsSIRT6 and HsSIRT4, respectively. Moreover, the homology found between the unique Ig-like domain comprised in AtSRT1 and the human GAS41 protein suggests that the function of this domain is to facilitate AtSRT1 interaction with specific substrates, possibly with similar features to those recognized by GAS41. Since protein domains that are fused in a single gene in a species are generally interaction and functional partners in species where they are encoded by different genes, the observation that the AtSRT1 sirtuin domain is fused to a GAS41-like domain in *Arabidopsis* indicates that HsSirt6 and GAS41, although encoded by different genes, may be interaction and functional partners in human as well.

Interestingly, SRT1 and SRT2 have higher 3D structure conservation and sequence identity with each other than SIRT6 and SIRT4, respectively, both within the catalytic domain and over the whole sequences, suggesting that the two *Arabidopsis* proteins are closer relatives than

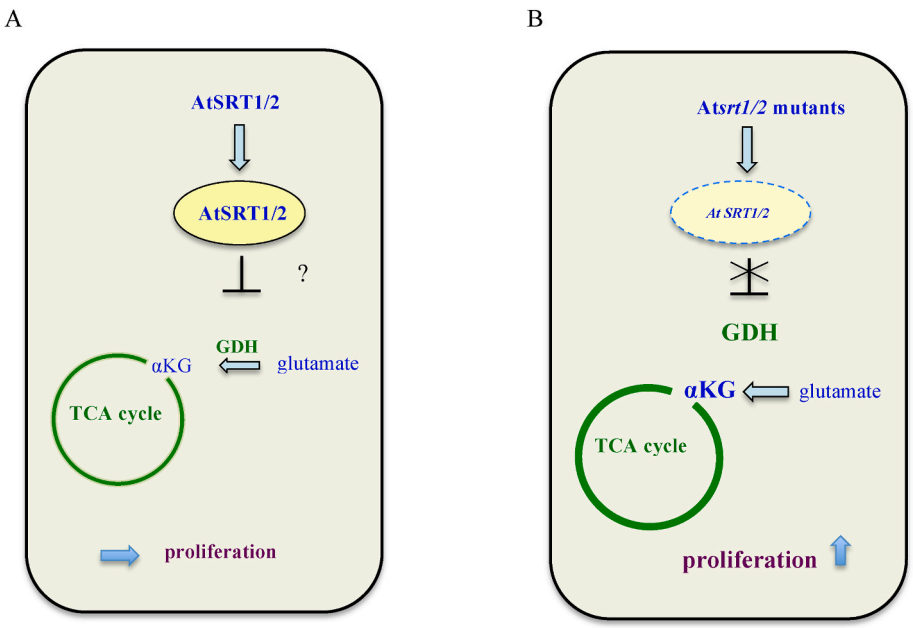

Fig. 6. Schematic representation of the putative effect of the two *Arabidopsis* sirtuins on GDH-mediated metabolism. A: WT plants. B: sirtuin mutant plants.

their human counterparts. This observation agrees with the similar effects exerted by SRT1 and SRT2 on plant proliferation and GDH activity.

The involvement of both the *Arabidopsis* sirtuins in the same process with similar effect is quite intriguing. Indeed, animal sirtuins are known to take part in proliferation by exerting distinct effects (Carafa et al., 2019). Additionally, human SIRT4 and SIRT3 are both able to regulate GDH activity, but with opposite results, i.e., inhibition and stimulation, respectively. Plant sirtuins are also known to exert different effects, and only in one previous report on ethylene pathway modulation the two *Arabidopsis* sirtuins have been shown to have a concordant role (Zhang et al., 2018).

In each sirtuin mutant we found a transcriptional decrease of the other sirtuin gene, indicating that AtSRT1 and AtSRT2 are interdependent, at least at a transcriptional level. In a previous report, an interdependence of the two sirtuins was also observed, although in that case an increase of the other sirtuin was observed in each mutant plant (Zhang et al., 2018). These data indicate that the relationship between AtSRT1 and AtSRT2 transcription is not univocal but may vary depending on the plant developmental state and experimental context.

In summary, this work demonstrates, for the first time, that *Arabidopsis* thaliana sirtuins are involved in cell proliferation, by exerting an inhibitory role that we suggest could mediated by inhibition of GDH activity, as observed for SIRT4 in mammalian cells, implicating a common trans-kingdom metabolic role. The proposed mechanism by which *Arabidopsis* sirtuins exert a GDH-mediated control of TCA cycle, and hence of cell proliferation, is reported in the cartoon depicted in Fig. 6.

In consideration of the fundamental importance of DNA synthesis regulation for cell survival, plants might utilize different systems to control replication rate, fuelling or stopping energy in relation to specific needs. In this context, GDH control by sirtuins might be exploited by plants as a fine-tuning modulator to manage specific energy requirements such as those occurring during development or stress conditions.

The future challenge will be to valuate if, in *Arabidopsis,* sirtuins regulate GDH as the major or the unique mechanism to control energy production in the proliferation process. The use of different plant growth conditions and/or selected mutants could be the way to obtain an answer to this problem.

Author contributions statement

Giovannella Bruscalupi: Assay of proliferation and glutamate dehydrogenase activity**.** Conceptualization, Writing - Original Draft, Writing - Review & Editing. **Maria Luisa Mauro:** Mutant plant production and phenotypical plant analyses. Conceptualization, Writing - Original Draft, Writing - Review & Editing. **Cristina Maria Failla:** Expression level analysis by qRT-PCR. Conceptualization, Writing - Review & Editing. **Veronica Morea:** Supervision of bioinformatics analyses. Conceptualization, Writing - Review & Editing. **Patrizio Di Micco:** Bioinformatics analysis of sirtuin sequences and residue conservation. **Gianmarco Pascarella:** Modelling, analysis and comparison of sirtuin 3D structures. **Michele Saliola:** GDH isomer electrophoretic analysis. **Angelo De Paolis:** Contribution to selection of mutant plant.

Declaration of competing interest

The authors declare that they have no known competing financial interests or personal relationships that could have appeared to influence the work reported in this paper.

Data availability

All data used for this article are reported within the article

Acknowledgments

This research received grants from Ateneo 2015 and 2016 to G.B and M.L.M. Sapienza University of Rome (Italy) and PRIN 2017 2017483NH8_005 to V.M.

Appendix A. Supplementary data

Supplementary data to this article can be found online at https://doi.org/10.1016/j.plaphy.2022.11.007.

References

Altschul, S.F., Madden, T.L., Schäffer, A.A., Zhang, J., Zhang, Z., Miller, W., Lipman, D.J., 1997. Gapped BLAST and PSI-BLAST: a new generation of protein database search

programs. Nucleic Acids Res. 25 (17), 3389–3402. https://doi.org/10.1093/nar/25.17.3389.
Baiza, M., Seda, V., Spurna, V., 1989. The uptake of 3 H-thymidine and its transport in Datura stramonium L. Biol. Plantarum 28, 230–233. https://doi.org/10.1007/BF02894602.
Beemster, G.T., De Veylder, L., Vercruysse, S., West, G., Rombaut, D., Van Hummelen, P., Galichet, A., Gruissem, W., Inzé, D., Vuylsteke, M., 2005. Genome-wide analysis of gene expression profiles associated with cell cycle transitions in growing organs of Arabidopsis. Plant Physiol. 138 (2), 734–743. https://doi.org/10.1104/pp.104.053884.
Berman, H.M., Westbrook, J., Feng, Z., Gilliland, G., Bhat, T.N., Weissig, H., Shindyalov, I.N., Bourne, P.E., 2000. The protein data bank. Nucleic Acids Res. 28 (1), 235–242. https://doi.org/10.1093/nar/28.1.235.
Bheda, P., Jing, H., Wolberger, C., Lin, H., 2016. The substrate specificity of sirtuins. Annu. Rev. Biochem. 85, 405–429. https://doi.org/10.1146/annurev-biochem-060815-014537.
Bond, D.M., Dennis, E.S., Pogson, B.J., Finnegan, E.J., 2009. Histone acetylation, VERNALIZATION INSENSITIVE 3, FLOWERING LOCUS C, and the vernalization response. Mol. Plant 2 (4), 724–737. https://doi.org/10.1093/mp/ssp021.
Carafa, V., Rotili, D., Forgione, M., Cuomo, F., Serretiello, E., Hailu, G.S., Jarho, E., Lahtela-Kakkonen, M., Mai, A., Altucci, L., 2016. Sirtuin functions and modulation: from chemistry to the clinic. Clin. Epigenet. 8, 61. https://doi.org/10.1186/s13148-016-0224-3.
Carafa, V., Altucci, L., Nebbioso, A., 2019. Dual tumor suppressor and tumor promoter action of sirtuins in determining malignant phenotype. Front. Pharmacol. 10, 38. https://doi.org/10.3389/fphar.2019.00038.
Chang, H.C., Guarente, L., 2014. SIRT1 and other sirtuins in metabolism. Trends Endocrinol. Metabol. 25 (3), 138–145. https://doi.org/10.1016/j.tem.2013.12.001.
Chen, Z., Lin, J., Feng, S., Chen, X., Huang, H., Wang, C., Yu, Y., He, Y., Han, S., Zheng, L., Huang, G., 2019. SIRT4 inhibits the proliferation, migration, and invasion abilities of thyroid cancer cells by inhibiting glutamine metabolism. OncoTargets Ther. 12, 2397–2408. https://doi.org/10.2147/OTT.S189536.
Cho, H.J., Li, H., Linhares, B.M., Kim, E., Ndoj, J., Miao, H., Grembecka, J., Cierpicki, T., 2018. GAS41 recognizes diacetylated histone H3 through a bivalent binding mode. ACS Chem. Biol. 13 (9), 2739–2746. https://doi.org/10.1021/acschembio.8b00674.
Csibi, A., Fendt, S.M., Li, C., Poulogiannis, G., Choo, A.Y., Chapski, D.J., Jeong, S.M., Dempsey, J.M., Parkhitko, A., Morrison, T., Henske, E.P., Haigis, M.C., Cantley, L.C., Stephanopoulos, G., Yu, J., Blenis, J., 2013. The mTORC1 pathway stimulates glutamine metabolism and cell proliferation by repressing SIRT4. Cell 153 (4), 840–854. https://doi.org/10.1016/j.cell.2013.04.023.
Dittenhafer-Reed, K.E., Richards, A.L., Fan, J., Smallegan, M.J., Fotuhi Siahpirani, A., Kemmerer, Z.A., Prolla, T.A., Roy, S., Coon, J.J., Denu, J.M., 2015. SIRT3 mediates multi-tissue coupling for metabolic fuel switching. Cell Metabol. 21 (4), 637–646. https://doi.org/10.1016/j.cmet.2015.03.007.
Dubois, F., Tercé-Laforgue, T., Gonzalez-Moro, M.B., Estavillo, J.M., Sangwan, R., Gallais, A., Hirel, B., 2003. Glutamate dehydrogenase in plants: is there a new story for an old enzyme? Plant Physiol. Biochem. 41 (6–7), 575–576. https://doi.org/10.1016/S0981-9428(03)00075-5.
Fang, Y., Tang, S., Li, X., 2019. Sirtuins in metabolic and epigenetic regulation of stem cells. Trends Endocrinol. Metabol. 30 (3), 177–188. https://doi.org/10.1016/j.tem.2018.12.002.
Groat, R.G., Vance, C.P., 1981. Root nodule enzymes of ammonia assimilation in alfalfa (medicago sativa L.): developmental patterns and response to applied nitrogen. Plant Physiol. 67 (6), 1198–1203. https://doi.org/10.1104/pp.67.6.1198.
Grozinger, C.M., Chao, E.D., Blackwell, H.E., Moazed, D., Schreiber, S.L., 2001. Identification of a class of small molecule inhibitors of the sirtuin family of NAD-dependent deacetylases by phenotypic screening. J. Biol. Chem. 276, 38837–38843. https://doi.org/10.1074/jbc.M106779200.
Haigis, M.C., Mostoslavsky, R., Haigis, K.M., Fahie, K., Christodoulou, D.C., Murphy, A. J., Valenzuela, D.M., Yancopoulos, G.D., Karow, M., Blander, G., Wolberger, C., Prolla, T.A., Weindruch, R., Alt, F.W., Guarente, L., 2006. SIRT4 inhibits glutamate dehydrogenase and opposes the effects of calorie restriction in pancreatic beta cells. Cell 126 (5), 941–954. https://doi.org/10.1016/j.cell.2006.06.057.
Hollender, C., Liu, Z., 2008. Histone deacetylase genes in Arabidopsis development. J. Integr. Plant Biol. 50 (7), 875–885. https://doi.org/10.1111/j.1744-7909.2008.00704.x.
Huang, L., Sun, Q., Qin, F., Li, C., Zhao, Y., Zhou, D.X., 2007. Down-regulation of a SILENT INFORMATION REGULATOR2-related histone deacetylase gene, OsSRT1, induces DNA fragmentation and cell death in rice. Plant Physiol. 144 (3), 1508–1519. https://doi.org/10.1104/pp.107.099473.
Jeong, S.M., Xiao, C., Finley, L.W., Lahusen, T., Souza, A.L., Pierce, K., Li, Y.H., Wang, X., Laurent, G., German, N.J., Xu, X., Li, C., Wang, R.H., Lee, J., Csibi, A., Cerione, R., Blenis, J., Clish, C.B., Kimmelman, A., Deng, C.X., et al., 2013. SIRT4 has tumor-suppressive activity and regulates the cellular metabolic response to DNA damage by inhibiting mitochondrial glutamine metabolism. Cancer Cell 23 (4), 450–463. https://doi.org/10.1016/j.ccr.2013.02.024.
Jumper, J., Evans, R., Pritzel, A., et al., 2021. Highly accurate protein structure prediction with AlphaFold. Nature 596, 583–589. https://doi.org/10.1038/s41586-021-03819-2.
Kang, J., Dengler, N., 2002. Cell cycling frequency and expression of the homeobox gene ATHB-8 during leaf vein development in Arabidopsis. Planta 216, 212–219. https://doi.org/10.1007/s00425-002-0847-9.
König, A.C., Hartl, M., Pham, P.A., Laxa, M., Boersema, P.J., Orwat, A., Kalitventseva, I., Plöchinger, M., Braun, H.P., Leister, D., Mann, M., Wachter, A., Fernie, A.R., Finkemeier, I., 2014. The Arabidopsis class II sirtuin is a lysine deacetylase and interacts with mitochondrial energy metabolism. Plant Physiol. 164 (3), 1401–1414. https://doi.org/10.1104/pp.113.232496.
Li, M., Li, C., Allen, A., Stanley, C.A., Smith, T.J., 2012. The structure and allosteric regulation of mammalian glutamate dehydrogenase. Arch. Biochem. Biophys. 519 (2), 69–80. https://doi.org/10.1016/j.abb.2011.10.015.
Liu, X., Wei, W., Zhu, W., Su, L., Xiong, Z., Zhou, M., Zheng, Y., Zhou, D.X., 2017. Histone deacetylase AtSRT1 links metabolic flux and stress response in Arabidopsis. Mol. Plant 10 (12), 1510–1522. https://doi.org/10.1016/j.molp. 2017.10.010.
Lowry, O.H., Rosebrough, N.J., Karr, A.L., Randall, R.J., 1951. Protein measurement with the Folin phenol reagent. J. Biol. Chem. 193, 265–275.
Lu, Y., Xu, Q., Liu, Y., Yu, Y., Cheng, Z.-Y., Zhao, Y., Zhou, D.-X., 2018. Dynamics and functional interplay of histone lysine butyrylation, crotonylation, and acetylation in rice under starvation and submergence. Genome Biol. 19, 144. https://doi.org/10.1186/s13059-018-1533-y.
Marchi, L., Degola, F., Polverini, E., Tercé-Laforgue, T., Dubois, F., Hirel, B., Restivo, F. M., 2013. Glutamate dehydrogenase isoenzyme 3 (GDH3) of Arabidopsis thaliana is regulated by a combined effect of nitrogen and cytokinin. Plant Physiol. Biochem. 73, 368–374. https://doi.org/10.1016/j.plaphy.2013.10.019.
Melo Oliveira, R., Cunha Oliveira, I., Coruzzi, G., 1996. Arabidopsis mutant analysis and gene regulation define a nonredundant role for glutamate dehydrogenase in nitrogen assimilation. Proc. Natl. Acad. Sci. USA 93, 4718–4723. https://doi.org/10.1073/pnas.93.10.4718.
Miyashita, Y., Good, A.G., 2008. NAD(H)-dependent glutamate dehydrogenase is essential for the survival of Arabidopsis thaliana during dark-induced carbon starvation. J. Exp. Bot. 59 (3), 667–680. https://doi.org/10.1093/jxb/erm340.
O'Callaghan, C., Vassilopoulos, A., 2017. Sirtuins at the crossroads of stemness, aging, and cancer. Aging Cell 16 (6), 1208–1218. https://doi.org/10.1111/acel.12685.
Pandey, R., Müller, A., Napoli, C.A., Selinger, D.A., Pikaard, C.S., Richards, E.J., Bender, J., Mount, D.W., Jorgensen, R.A., 2002. Analysis of histone acetyltransferase and histone deacetylase families of Arabidopsis thaliana suggests functional diversification of chromatin modification among multicellular eukaryotes. Nucleic Acids Res. 30 (23), 5036–5055. https://doi.org/10.1093/nar/gkf660.
Pettersen, E.F., Goddard, T.D., Huang, C.C., Couch, G.S., Greenblatt, D.M., Meng, E.C., Ferrin, T.E., 2004. UCSF Chimera - a visualization system for exploratory research and analysis. J. Comput. Chem. 25, 1605–1612. https://doi.org/10.1002/jcc.20084.
Schlicker, C., Gertz, M., Papatheodorou, P., Kachholz, B., Becker, C.F., Steegborn, C., 2008. Substrates and regulation mechanisms for the human mitochondrial sirtuins Sirt3 and Sirt5. J. Mol. Biol. 382 (3), 790–801. https://doi.org/10.1016/j.jmb.2008.07.048.
Sievers, F., Wilm, A., Dineen, D., Gibson, T.J., Karplus, K., Li, W., Lopez, R., McWilliam, H., Remmert, M., Söding, J., Thompson, J.D., Higgins, D.G., 2011. Fast, scalable generation of high-quality protein multiple sequence alignments using Clustal Omega. Mol. Syst. Biol. 7, 539. https://doi.org/10.1038/msb.2011.75.
Tercé-Laforgue, T., Clement, G., Marchi, L., Restivo, F.M., Lea, P.J., Hirel, B., 2015. Resolving the role of plant NAD-glutamate dehydrogenase: III. Overexpressing individually or simultaneously the two enzyme subunits under salt stress induces changes in the leaf metabolic profile and increases plant biomass production. Plant Cell Physiol. 56, 1918–1929. https://doi.org/10.1093/pcp/pcv114.
Turano, F.J., Thakkar, S.S., Fang, T., Weisemann, J.M., 1997. Characterization and expression of NAD(H)-dependent glutamate dehydrogenase genes in Arabidopsis. Plant Physiol. 113 (4), 1329–1341. https://doi.org/10.1104/pp.113.4.1329.
Wang, C., Gao, F., Wu, J., Dai, J., Wei, C., Li, Y., 2010. Arabidopsis putative deacetylase AtSRT2 regulates basal defense by suppressing PAD4, EDS5 and SID2 expression. Plant Cell Physiol. 51 (8), 1291–1299. https://doi.org/10.1093/pcp/pcq087.
Wang, G., Köhler, C., 2017. Epigenetic processes in flowering plant reproduction. J. Exp. Bot. 68 (4), 797–807. https://doi.org/10.1093/jxb/erw486.
Wang, Y.Q., Wang, H.L., Xu, J., Tan, J., Fu, L.N., Wang, J.L., Zou, T.H., Sun, D.F., Gao, Q. Y., Chen, Y.X., Fang, J.Y., 2018. Sirtuin5 contributes to colorectal carcinogenesis by enhancing glutaminolysis in a deglutarylation-dependent manner. Nat. Commun. 9 (1), 545. https://doi.org/10.1038/s41467-018-02951-4.
Zhang, F., Wang, L., Ko, E.E., Shao, K., Qiao, H., 2018. Histone deacetylases SRT1 and SRT2 interact with ENAP1 to mediate ethylene-induced transcriptional repression. Plant Cell 30 (1), 153–166. https://doi.org/10.1105/tpc.17.00671.
Zhang, H., Zhao, Y., Zhou, D.X., 2017. Rice NAD+-dependent histone deacetylase OsSRT1 represses glycolysis and regulates the moonlighting function of GAPDH as a transcriptional activator of glycolytic genes. Nucleic Acids Res. 45 (21), 12241–12255. https://doi.org/10.1093/nar/gkx825.
Zhang, J., Pavlova, N.N., Thompson, C.B., 2017. Cancer cell metabolism: the essential role of the nonessential amino acid, glutamine. EMBO J. 36 (10), 1302–1315. https://doi.org/10.15252/embj.201696151.
Zheng, W., 2020. Review: the plant sirtuins. Plant Sci. 293, 110434 https://doi.org/10.1016/j.plantsci.2020.110434.
Zhong, X., Zhang, H., Zhao, Y., Sun, Q., Hu, Y., Peng, H., Zhou, D.-X., 2013. The rice NAD (+)-dependent histone deacetylase OsSRT1 targets preferentially to stress- and metabolism-related genes and transposable elements. PLoS One 8, e66807. https://doi.org/10.1371/journal.pone.0066807.